Acetylcholine Binding Site in the Vesicular Acetylcholine Transporter[†]

Ana M. Ojeda, Natalia G. Kolmakova, and Stanley M. Parsons*

Department of Chemistry and Biochemistry and Neuroscience Research Institute, University of California, Santa Barbara, California 93106-9510

Received March 4, 2004; Revised Manuscript Received June 21, 2004

ABSTRACT: This study sought primarily to locate the acetylcholine (ACh) binding site in the vesicular acetylcholine transporter (VAChT). The design of the study also allowed us to locate residues linked to (a) the binding site for the allosteric inhibitor vesamicol and (b) the rates of the two transmembrane reorientation steps of a transport cycle. In more characterized proteins, ACh is known to be bound in part through cation−π solvation by tryptophan, tyrosine, and phenylalanine residues. Each of 11 highly conserved W, Y, and F residues in putative transmembrane domains (TMDs) of rat VAChT was mutated to A and a different aromatic residue to test for loss of cation−π solvation. Mutated VAChTs were expressed in PC12$^{A123.7}$ cells and characterized with the goal of determining whether mutations widely perturbed structure. The thermodynamic affinity for ACh was determined by displacement of trace [^{3}H]-(−)-*trans*-2-(4-phenylpiperidino)cyclohexanol (vesamicol) with ACh, and Michaelis−Menten parameters were determined for [^{3}H]ACh transport. Expression levels were determined with [^{3}H]vesamicol saturation curves and Western blots, and they were used to normalize V_{max} values. "Microscopic" parameters for individual binding and rate steps in the transport cycle were calculated on the basis of a published kinetics model. All mutants were expressed adequately, were properly glycosylated, and bound ACh and vesamicol. Subcellular mistargeting was shown not to be responsible for poor transport by some mutants. Mutation of residue W331, which lies in the beginning of TMD VIII proximal to the vesicular lumen, produced 5- and 9-fold decreased ACh affinities and no change in other parameters. This residue is a good candidate for cation−π solvation of bound ACh. Mutation of four other residues decreased the ACh affinity up to 6-fold and also affected microscopic rate constants. The roles of these residues in ACh binding and transport thus are complex. Nine mutations allowed us to resolve the ACh and vesamicol binding sites from each other. Other mutations affected only the rates of the transmembrane reorientation steps, and four mutations *increased* the rate of one or the other. Two mutations increased the value of K_M up to 5-fold as a result of rate effects with no ACh affinity effect. The results demonstrate that analysis of microscopic kinetics is required for the correct interpretation of mutational effects in VAChT. Results also are discussed in terms of recently determined three-dimensional structures for other transporters in the major facilitator superfamily.

Storage of acetylcholine (ACh)[1] by synaptic vesicles is mediated by the vesicular acetylcholine transporter (VAChT), which is driven by proton-motive force generated by V-ATPase (*1*−*3*). Alfonso *et al.* (*4*) were the first to clone VAChT. Predicted sequences now are available for many species (*5*−*12*). Hydropathy analysis indicates that VAChT contains 12 putative transmembrane domains (TMDs), with N- and C-termini exposed to the cytoplasm. The location of the ACh binding site is unknown.

After discovering a synthetic receptor with a strong affinity for ACh (*13*), Dougherty *et al.* (*14*) proposed a novel model for binding sites that are selective for ACh and choline. They hypothesized that electron-rich aromatics can effectively and selectively solvate the quaternary ammonium functional group through cation−π interaction (binding of an organic cation to π-electrons in aromatic rings). The interaction is a complex phenomenon involving charge-dipole, charge-quadrupole, charge-induced dipole, π-polarization, and other effects (*15*). Tryptophan, tyrosine, and phenylalanine side chains can engage in this interaction. The magnitude and generality of the effect have been established by computation (*16*, *17*), gas-phase measurements (*18*, *19*), and characterization of model receptors in water (*20*, *21*).

Several relevant crystal structures and chemical studies of proteins are available. The Fab fragment McPC603 binds phosphocholine using the face of a tryptophan to contact the choline headgroup (*22*). ACh esterase (AChE, EC 3.1.1.7) often is considered the foremost example of cation−π

[†] This research was supported by Grant NS15047 from the National Institute of Neurological Disorders and Stroke.

* To whom all correspondence should be addressed: Department of Chemistry and Biochemistry, University of California, Santa Barbara, CA 93106-9510. E-mail: parsons@chem.ucsb.edu. Telephone: (805) 893-2252. Fax: (805) 893-4120.

[1] Abbreviations: ACh, acetylcholine; VAChT, vesicular acetylcholine transporter; vesamicol (formerly AH5183), (−)-*trans*-2-(4-phenylpiperidino)cyclohexanol; VMAT, vesicular monoamine transporter; B_{max}, maximal concentration of vesamicol binding sites; K_v, dissociation constant for vesamicol; K_{ACh}, thermodynamic dissociation constant for ACh; K_M, Michaelis−Menten constant for ACh transport; V_{max}, maximal velocity of transport; LacY, lactose permease; MFS, major facilitator superfamily; AChE, ACh esterase; PBS, phosphate-buffered saline; SDS, sodium dodecyl sulfate; SYPH, synaptophysin; TMD, transmembrane domain; UBB, uptake/binding buffer.

10.1021/bi049562b CCC: $27.50
Published on Web 08/10/2004

Table 1: Primers Used for Mutagenesis[a]

mutant	primer[b]
Y50A	5′-GGACAACATGTTG**GCC**ATGGTCATCGTGCCCATTGTTCC-3′
Y50F	5′-GGACAACATGTTG**TTC**ATGGTCATCGTGCCCATTGTTCC-3′
Y175A	5′-GCCTTTGCAGAAGAC**GCT**GCCACGCTCTTCGCTGCGCG-3′
Y175F	5′-GCCTTTGCAGAAGAC**TTT**GCCACGCTCTTCGCTGCGCG-3′
F191A	5′-CCTGGGCTCGGCC**GCC**GCGGACACGTCTGG-3′
F191Y	5′-CCTGGGCTCGGCC**TAC**GCGGACACGTCTGG-3′
F220A	5′-GGCGTGGCGCTAGCC**GCC**ATTAGCTTTGGAAGCC-3′
F220Y	5′-GGCGTGGCGCTAGCC**TAC**ATTAGCTTTGGAAGCC-3′
F223A	5′-CTAGCCTTTATTAGC**GCC**GGAAGCCTAGTGGCGCC-3′
F223Y	5′-CTAGCCTTTATTAGC**TAC**GGAAGCCTAGTGGCGCC-3′
F307A	5′-CATTCCCCTTGCG**GCC**CTCGAGCCCACC-3′
F307Y	5′-CATTCCCCTTGCG**TAC**CTCGAGCCCACC-3′
W331A	5′-GGGAGATGGGCATGGTT**GCC**CTGCCGGCTTTCGTGCC-3′
W331F	5′-GGGAGATGGGCATGGTT**TTC**CTGCCGGCTTTCGTGCC-3′
F335A	5′-GGTTTGGCTGCCGGCT**GCC**GTGCCACACGTGTTAGG-3′
F335Y	5′-GGTTTGGCTGCCGGCT**TAC**GTGCCACACGTGTTAGG-3′
Y343A	5′-CACGTGTTAGGCGTC**GCC**CTCACCGTGCGCCTGG-3′
Y343F	5′-CACGTGTTAGGCGTC**TTC**CTCACCGTGCGCCTGG-3′
Y428A	5′-GCCATAGCTGACATCTCC**GCT**TCTGTGGCCTACGCGCTCGG-3′
Y428F	5′-GCCATAGCTGACATCTCC**TTT**TCTGTGGCCTACGCGCTCGG-3′
Y432A	5′-CCTATTCTGTGGCC**GCC**GCGCTCGGGCCC-3′
Y432F	5′-CCTATTCTGTGGCC**TTC**GCGCTCGGGCCC-3′

[a] Forward primers are listed. [b] The mutant codon is underlined and in boldface.

solvation in biological systems. Virtual docking of ACh with the active site of AChE places the quaternary ammonium group in van der Waals contact with a tryptophan (*23*). Results from both X-ray crystallography and photoaffinity labeling using a number of quaternary ammonium ligands assign phenylalanine to the "anionic subsite" of the active site and tryptophan to the "peripheral anionic site" of AChE (*24*). A soluble molluscan protein related to the nicotinic ACh receptor has aromatic residues lining the ACh binding site (*25*). Moderate-resolution structure, photoaffinity labeling, and unnatural amino acid methodology have revealed that the nicotinic ACh receptor contains a number of aromatic residues engaged in cation$-\pi$ solvation of ACh (*26*−*28*). On the basis of structural analysis and site-directed mutagenesis, Schiefner *et al*. (*29*) described interaction between the quaternary ammonium group of the substrate betaine and the indole groups of three tryptophans in the binding pocket of ABC transporter ProU from *Escherichia coli*.

Thus, structural and chemical results make it clear that tryptophan, tyrosine, and phenylalanine residues might be located in the ACh binding site of VAChT. It is likely that such residues are conserved. Moreover, binding sites for transporter substrates are expected to be located in TMDs (*30*). A large number of aromatics in putative TMDs of VAChT are conserved. Many of these are likely to be important to protein folding and not the ACh binding site. How can such residues be eliminated from the list of candidates? VAChT is closely related to vesicular monoamine transporters 1 and 2 (VMATs), which have substrates containing a primary or secondary amine. Cation$-\pi$ solvation is much less effective for primary and secondary amines than for quaternary amines (*31*). Thus, VMATs probably will not conserve aromatic residues at positions corresponding to those binding the quaternary ammonium of ACh in VAChT.

This hypothesis led to a focus on conserved aromatics in putative TMDs of VAChT that are not conserved in VMATs. VAChT was mutated at these residues and transiently expressed. Relevant properties of the mutants were determined, and the results are reported and interpreted in this paper.

MATERIALS AND METHODS

Materials. The PC12$^{A123.7}$ mutant pheochromocytoma PC12 cell line (*32*) was obtained from L. Hersh (University of Kentucky, Lexington, KY). This cell line is deficient in both type I and type II cAMP-dependent PKA activity, and choline acetyltransferase (*33*) and VAChT (*34*) activities are barely detectable. PC12$^{A123.7}$ cells contain synaptic-like microvesicles to which VAChT is targeted (*35*).

Mutagenesis. Rat VAChT cDNA subcloned into the expression vector pcDNA3.1D/V5-His-TOPO without a poly-H tag was obtained as a gift from D. T. Bravo. Primers for mutagenesis were synthesized commercially (Table 1). Site-directed mutagenesis was performed using the QuikChange mutagenesis kit (Stratagene, La Jolla, CA). Mutagenesis was performed according to the manufacturer's instructions. Wild-type and mutant plasmids were purified from XL1Blue cells (Stratagene) using a DNA purification kit (Qiagen, Valencia, CA). Wild-type and mutated VAChTs were sequenced using the Thermo Sequenase radiolabeled terminator cycle sequencing kit (USB, Cleveland, OH).

Transient Expression. PC12$^{A123.7}$ cells were maintained at 37 °C in an atmosphere of 10% CO_2 in complete Dulbecco's modified Eagle's medium nutrient mixed 1:1 with Ham's F-12 medium. The culture medium was supplemented with 5% heat-inactivated horse serum, 10% fetal bovine serum, 100 units/mL penicillin, and 100 μg/mL streptomycin. Wild-type and mutated VAChT cDNAs were transiently transfected into PC12$^{A123.7}$ cells by electroporation as described previously (*36*). The parent vector (Invitrogen, Carlsbad, CA) was transfected in parallel as a negative control. Briefly, cells were detached with trypsin, washed, and resuspended in cold phosphate-buffered saline (PBS) at a cell density of $\sim 6 \times 10^7$ cells/mL. Resuspended cells were mixed with DNA (50−100 μg), electroporated at 0.2 kV and 1.4 mF, and replated in the medium described above. Transfected cells were harvested 72 h after electroporation.

Preparation of Postnuclear Supernatants. Vesicle-containing postnuclear supernatants were prepared as described previously (*36*). Briefly, transfected cells were harvested, washed with cold PBS, and resuspended in homogenization buffer [10 mM *N*-(2-hydroxyethyl)piperazine-*N*′-2-ethanesulfonic acid (HEPES) adjusted to pH 7.4 with KOH and 0.32 M sucrose] supplemented with protease inhibitors. Cells were broken in a Potter-Elvehjam homogenizer until 95% of them took up trypan blue as determined by microscopic examination (three to six strokes), and the resulting suspension was centrifuged at 800*g* for 10 min. The protein concentration in the postnuclear supernatant was estimated with the Bradford protein assay (Bio-Rad, Hercules, CA). The supernatant was incubated with 100 μM diethyl *p*-nitrophenylphosphate (paraoxon, Sigma-Aldrich, St. Louis, MO) for 30 min at 23 °C to inhibit AChE activity, divided into portions, quick-frozen, and stored at −80 °C until it was used.

SDS−Polyacrylamide Gel Electrophoresis and Western Blot Analysis. Expression of wild-type and mutated VAChT was monitored by Western blot analysis as described by Kim *et al*. (*37*) with some modifications. Fifty micrograms of protein was diluted to 500 μL with homogenization buffer containing complete protease inhibitor cocktail (Roche, Nutley, NJ) and pelleted by centrifugation at 100000*g* for 2 h at 4 °C. The pellet was resuspended in 200 μL of 1× SDS sample buffer (New England BioLabs, Beverly, MA) containing 0.42 M dithiothreitol. Proteins were separated by electrophoresis on a 10% SDS−polyacrylamide gel and blotted onto an Invitrolon PVDF membrane (Invitrogen) using a semidry electrotransfer apparatus (E&K, Saratoga, CA). The membrane then was blocked with Tris-buffered saline (TBS) containing 2.5% nonfat milk and 0.05% Tween 20 for 1 h at 23 °C, followed by incubation with polyclonal goat antibody raised against the N-terminus of human VAChT (Santa Cruz Biotechnology, Santa Cruz, CA). Membranes were rinsed and incubated for 1 h with horseradish peroxidase-conjugated donkey anti-goat IgG (Santa Cruz Biotechnology) at 23 °C. Electrochemiluminescent (ECL) detection was performed using a standard kit (Santa Cruz Biotechnology) as instructed by the manufacturer.

Vesamicol Binding Assay. Vesamicol binding was carried out according to the method of Kim *et al*. (*37*) with some modifications. The postnuclear supernatant (100 μg of protein) was mixed with uptake/binding buffer (UBB) [110 mM potassium tartrate, 20 mM HEPES (pH 7.4 with KOH), and 1 mM ascorbic acid] to yield a final volume of 200 μL containing the stated concentration of [^{3}H]vesamicol. Incubation was continued for 30 min at 37 °C. Polyethyleniminecoated glass fiber filters (type GF/F, Whatman, Clifton, NJ) were prewashed with cold UBB using vacuum-assisted filtration. Two 90 μL portions of the vesicular suspension at each concentration of [^{3}H]vesamicol were filtered, and unbound radioactivity was removed immediately from each sample with four 1 mL washes with ice-cold UBB. Radioactivity bound to the filters was estimated by liquid scintillation spectrometry in 3.5 mL of Bio-Safe II (Research Products International, Mt. Prospect, IL). Nonspecific binding was assessed in the presence of radiolabeled ligand and 4 μM unlabeled vesamicol (*36*). Data for duplicates were averaged. The equations $B_{ns} = m \times \mathrm{Ves} + b$ and $B_t = B_{ns} + (B_{max} \times \mathrm{Ves})/(K_v + \mathrm{Ves})$, where B_{ns} is the amount of nonspecifically bound vesamicol, m is the slope of nonspecific binding, Ves is the concentration of [^{3}H]vesamicol, b is the intercept for nonspecific binding, B_t is the total amount of bound vesamicol, B_{max} is the concentration of specific vesamicol binding sites, and K_v is the vesamicol dissociation constant, were simultaneously fit to averaged data. The fitted level of nonspecific binding was subtracted from data before plotting.

Acetylcholine Dissociation Constant. The ACh dissociation constant was estimated by assessing the competition between ACh and binding of tracer [^{3}H]vesamicol. Dry ACh chloride (1.63 g, Sigma-Aldrich) was rapidly dissolved in paraoxon-treated UBB and brought to 4.00 mL in a volumetric flask to make a 2.25 M stock solution. Aliquots of the postnuclear supernatant containing 250 μg of protein were mixed with paraoxon-treated UBB and different concentrations of unlabeled ACh and incubated for 10 min at 37 °C. After this, a final [^{3}H]vesamicol concentration of 5 nM was added, and incubation was continued for 10 min at 37 °C. Bound radioactivity in two 90 μL portions at each concentration of ACh was determined by filtration as described above. The level of nonspecific binding was determined in the presence of 4 μM unlabeled vesamicol. Data for duplicates were averaged. Use of trace [^{3}H]vesamicol means the IC_{50} value for displacement will be essentially equal to the equilibrium dissociation constant K_{ACh}. Thus, the equations $B_{ns} = b$ and $B_t = b + B_0 K_{ACh}{}^H/(K_{ACh}{}^H + \mathrm{ACh}^H)$ were fit simultaneously to data for nonspecific and total binding, respectively, where B_{ns} is the amount of nonspecifically bound [^{3}H]vesamicol, b is the intercept for nonspecific binding of slope 0, B_t is the total amount of bound [^{3}H]vesamicol, B_0 is the amount of specifically bound [^{3}H]vesamicol in the absence of ACh, K_{ACh} is the ACh dissociation constant, H is the Hill coefficient, and ACh is the concentration of ACh. To test the necessity of an adjustable Hill coefficient, the software S-Plus (Insightful Corp., Seattle, WA) was used to perform the likelihood ratio test (*38*, *39*). The fitted level of nonspecific binding was subtracted from data before plotting.

Acetylcholine Transport Assay. Transport was assessed in a manner similar to that of Kim *et al*. (*37*) with some modifications. [^{3}H]ACh (76−82 mCi/mmol, Perkin-Elmer, Wellesley, MA) was diluted with unlabeled ACh to make a 25 mCi/mmol stock solution. The postnuclear supernatant (250 μg of protein) was mixed with paraoxon-treated UBB to a final volume of 200 μL containing 10 mM Mg^{2+}ATP, 2 mM $MgCl_2$, 1 mM EDTA, and the stated concentration of [^{3}H]ACh. Transport was allowed to proceed for 10 min at 37 °C. It was terminated by diluting a 90 μL portion into 1 mL of ice-cold paraoxon-treated UBB in duplicate. Diluted samples were filtered and washed, and bound radioactivity was solubilized in 0.35 mL of 1% SDS. Filters were incubated with occasional shaking for 1 h, after which 3.5 mL of scintillation cocktail was added, and radioactivity was quantitated as previously described. The level of nonspecific transport was determined in the presence of 4 μM unlabeled vesamicol. Data for duplicates were averaged. The equations $V_{ns} = m \times \mathrm{ACh} + b$ and $V_t = V_{ns} + (V_{max} \times \mathrm{ACh})/(K_M + \mathrm{ACh})$, where V_{ns} is the amount of nonspecific transport, m is the slope of nonspecific transport, ACh is the concentration of [^{3}H]ACh, b is the intercept for nonspecific transport, V_t is the total amount of ACh taken up, V_{max} is the maximal amount of specific transport, and K_M is the Michaelis−

Menten constant for ACh transport, were simultaneously fit to averaged data. The extent of specific transport was obtained by subtracting the calculated extent of nonspecific transport from the experimentally determined extent of total uptake. The extent of specific transport was divided by B_{max} for the same preparation of postnuclear supernatant to obtain the number of molecules of ACh taken up *per* molecule of transporter over the time period of the experiment. "Normalized" data then were fit with a rectangular hyperbola to estimate values of normalized turnover V_{max}/B_{max} and K_M.

For those mutants showing little transport, errors associated with V_{max} and K_M are too large to permit regression to separated values. The data also usually did not exhibit saturation. In these cases, the V_{max}/K_M ratio was fit to the level of total transport using the equations $V_{ns} = m \times \text{ACh} + b$ and $V_t = V_{ns} + \text{ratio} \times \text{ACh}$, where ratio $= V_{max}/K_M$. The extent of specific transport was normalized as described above to estimate $V_{max}/B_{max}/K_M$, which is the apparent second-order rate constant for transport at ACh concentrations much lower than K_M.

Immunofluorescence. Cells were grown on collagen-coated glass coverslips (Becton Dickinson, Franklin Lakes, NJ) and fixed with 4% paraformaldehyde and 0.1% glutaraldehyde in PBS for 30 min at 4 °C. Blocking was performed for 1 h at 23 °C in immunofluorescence (IF) buffer [PBS (pH 7.4) containing 0.02% saponin (Sigma-Aldrich) and 5% donkey serum (Jackson Immunoresearch Laboratories, West Grove, PA)]. Cells were incubated with primary antibodies [1:50 for VAChT and 1:100 for synaptophysin (SYPH)] diluted in IF buffer for 1 h at 23 °C, washed three times for 10 min each in IF buffer, incubated for an additional 1 h with the appropriate secondary antibodies diluted in IF buffer, and washed again three times for 10 min each. To detect the VAChT primary antibody (Santa Cruz Biotechnology), the secondary antibody (1:100 dilution) was a donkey anti-goat antibody conjugated to Cy2 (Jackson Immunoresearch Laboratories). For the antibodies to SYPH (Santa Cruz Biotechnology), donkey anti-rabbit antibodies (1:200 dilution) conjugated to Cy3 were used (Jackson Immunoresearch Laboratories). After being washed, the coverslips were mounted onto glass slides, and the staining was then visualized with a Bio-Rad 1024 MRC laser scanning confocal system coupled to a Nikon Diaphot microscope with an oil immersion objective (60×). The appropriate set of filters and laser lines was used to avoid bleed-through between red and green fluorescence. Images were processed using Lasersharp (Bio-Rad) and Adobe Photoshop (Adobe Systems, Inc., Mountain View, CA).

Statistical Analysis. Isotherms for ACh displacement and vesamicol binding and the saturation curve for ACh transport were determined for the wild type and every mutant. Values for macroscopic parameters describing the outcomes of these assays were estimated by regression using Scientist (MicroMath Research, St. Louis, MO). To test reproducibility and obtain sufficient numbers of replicates to determine whether mutants differ from the wild type in an assay property, each type of assay was conducted two or more times on each VAChT species, except as noted (footnote g in Table 3). The more abnormal a mutant appeared, the more times it was assayed. Replicate values for macroscopic parameters were averaged, and standard deviations for the replicates were used to estimate the standard deviation of the mean according to eq 1.

$$Y \pm \sigma_Y = \frac{A + B + ...}{n} \pm \frac{\sqrt{\sigma_A^2 + \sigma_B^2 + ...}}{n} \quad (1)$$

where Y is the mean of replicate values for a macroscopic parameter (for example, K_M), σ_Y is the estimated standard deviation associated with Y, A, B, ..., etc., are the replicate values for the parameter, n is the number of replicates, and σ_A, σ_B, ..., etc., are the standard deviations corresponding to A, B, ..., etc., respectively.

To assess whether a parameter value (K_{ACh}, K_v, K_M, V_{max}/B_{max}, $V_{max}/B_{max}/K_M$, k_2, and k_1) for a mutant differs from that for the wild type, eq 2 was used.

$$\Delta Z \pm 3\sigma_{\Delta Z} = (Z_{WT} - Z_{MUT}) \pm 3\sqrt{\sigma_{Z_{WT}}^2 + \sigma_{Z_{MUT}}^2 + ...} \quad (2)$$

where ΔZ is the difference between the values of the parameter for the wild type and mutant, $3\sigma_{\Delta Z}$ is 3 times the propagated standard deviation associated with ΔZ, Z_{WT} and Z_{MUT} are the values of the parameter for the wild type and mutant, respectively, and $\sigma_{Z_{WT}}$ and $\sigma_{Z_{MUT}}$ are the propagated standard deviations associated with Z_{WT} and Z_{MUT}, respectively. If the interval $\Delta Z \pm 3\sigma_{\Delta Z}$ contains 0 (null interval), then the mutant and wild-type values for the parameter are considered the same within error. Otherwise, they are different. A mutant was not considered notably different from the wild type unless a parameter value *also* was at least 2-fold different. Values of macroscopic parameters meeting both criteria are shown in boldface in Tables 2 and 3, except for B_{max}, the variation of which is not intrinsically interesting in the current work.

RESULTS

Site-Directed Mutagenesis, Transient Expression, and Vesicle Preparation. Ten conserved W, Y, and F residues in putative TMDs of rat VAChT are not conserved in closely related VMATs (Figure 1). Each such residue in rat VAChT was mutated to alanine and a different aromatic residue. One Y conserved in VAChT and VMATs was mutated as a control, for a total of 22 mutants produced. The mutants were transiently expressed in a variant of PC12 cells that (a) expresses essentially no endogenous VAChT and (b) contains synaptic-like microvesicles to which VAChT is targeted (*34*, *35*). Expressing cells were homogenized and centrifuged to prepare the postnuclear supernatant containing VAChT in microvesicles.

Wild-type and mutant transporters were characterized by Western blot analysis (Figure 2). They all migrated as diffuse bands with an apparent molecular mass of approximately 85 kDa (arrow). This value is greater than that predicted for the polypeptide (56.5 kDa) because of glycosylation. Thus, all of the mutants were properly glycosylated and not apparently differentially degraded by proteases. Expression levels of mutants estimated from staining intensity often differed from that of wild-type VAChT. The differences are likely to be due to changes in mRNA stability and/or the success of protein folding during insertion into the endoplasmic reticulum (*40*).

TMD #	I	III	IV	V	V	VII	VIII	VIII	VIII	XI	XI
Rat residue #	Y50	Y175	F191	F220	F223	F307	W331	F335	Y343	Y428	Y432
Rat	LYM	DYA	AFA	AFI	SFG	AFL	VWL	AFV	VYL	SYS	AYA
Mouse	LYM	DYA	AFA	AFI	SFG	AFL	VWL	AFV	VYL	SYS	AYA
Human	LYM	DYA	AFA	AFI	SFG	AFL	AWL	AFV	VYL	SYS	AYA
T. californica	LYM	SYA	AFA	AFI	SFG	AFL	TWL	AFF	VYI	SYS	AYA
D. rerio	LYM	NYG	AFA	AFI	SFG	AFL	VWL	AFL	VYI	SYS	AYA
C. intestinalis	LYM	GFA	ALA	AFI	SFG	AFL	VWL	AFL	VYL	SYS	AYS
Drosophila	LYM	SYS	AFA	AFI	SFG	AFL	VWL	AFF	VVI	SYS	AYA
L. stagnalis	LYM	SYA	AFA	AFI	SFG	AFL	CWL	SFV	VYM	SYS	AYA
C. elegans	LYM	SYG	AFA	AFI	SFG	AFL	IWL	PFF	VYV	SYS	AYA
VMAT1	MLT	TY-	SFS	GGL	ALG	AIL	AFL	ASV	TNL	AFC	-FA
VMAT2	LLT	SYA	SCS	GGL	AMG	AML	AFL	ASI	TNI	AFC	GYA

FIGURE 1: Mutated residues (shaded) in rat VAChT. The Roman numeral of the putative TMD containing the residue (TMD #) and the Arabic number of the residue in the rat sequence (Rat residue #) are shown at the top. Sequences at the sites of mutation are shown for nine species of VAChT (*Caenorhabditis elegans* NCBI protein accession number P34711, *Drosophila* NCBI protein accession number O17444, great pond snail *Lymnaea stagnalis* NCBI protein accession number AAO83850, *Ciona intestinalis* NCBI protein accession number BAB85860, zebrafish *Danio rerio* NCBI protein accession number P59845, marine ray *Torpedo* NCBI protein accession number P81721, mouse NCBI protein accession number O35304, rat NCBI protein accession number Q62666, and human NCBI protein accession number Q16572). Consensus sequences (more than two-thirds identical) for VMAT1 and VMAT2 are shown below the VAChT alignments. A residue position in VMATs not exhibiting consensus is denoted with a dash.

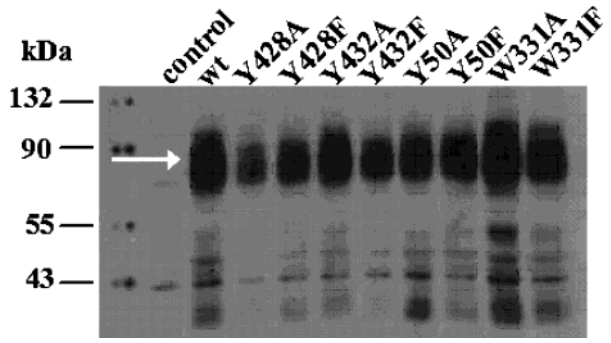

FIGURE 2: Western blot analysis of wild-type and mutant rat VAChTs. Membranes in approximately 50 μg of the postnuclear supernatant were analyzed. All VAChTs appeared as diffuse bands with a molecular mass of 85 kDa due to glycosylation (white arrow). Mass standards are given at the left.

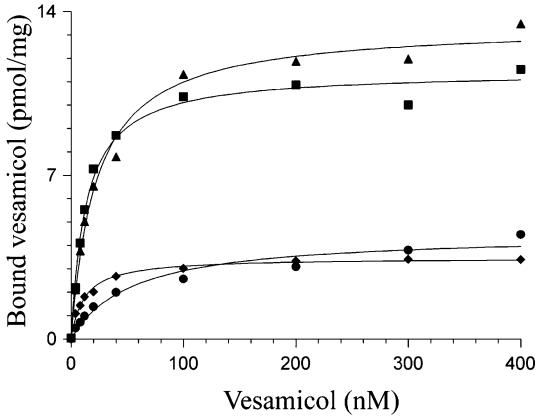

FIGURE 3: Vesamicol saturation curves. The postnuclear supernatant was incubated at the indicated concentrations of [^{3}H]vesamicol and then filtered and washed. Data are for representative experiments using wild-type (■), F335A (●), F220Y (▲), and Y428A (◆) VAChT. Transfection efficiency in individual experiments varied significantly.

Vesamicol Saturation Curves. Vesamicol inhibits VAChT by binding to an allosteric site on the outside of the vesicle (*41*−*46*). It has nanomolar affinity and can be used in radioactive form to titrate the amount and affinity of mutant VAChT. Knowledge of the amount of VAChT present in a preparation of the postnuclear supernatant is required to normalize the rate of [^{3}H]ACh transport to the expression level. Representative data are shown in Figure 3, and parameters for saturation curves fitted to such data for wild-type and all mutated VAChTs are listed in Table 2. The K_v value for the wild type is 14.3 ± 0.5 nM. Conservative and nonconservative mutations had little effect on vesamicol affinity (less than 2-fold) with the exception of the F335A mutation, which increased the dissociation constant to 38.4 ± 3.1 nM. B_{max} values obtained for different mutants differed greatly from each other but were approximately reproducible (Table 2). They correlated with different expression levels observed by Western blot analysis.

ACh Dissociation Constant. ACh inhibits binding of [^{3}H]vesamicol, even though ACh and vesamicol bind to nonidentical sites (see below). The phenomenon can be used to determine whether a mutation alters equilibrium affinity for ACh. If it does, the mutation alters the structure of the ACh binding site. Representative data for displacement of trace [^{3}H]vesamicol by unlabeled ACh are shown in Figure 4, and parameters for displacement curves fitted to such data for the wild type and all mutated VAChTs are listed in Table 2. Different expression levels do not affect the accuracy of determined K_{ACh} values. The data for the wild type and all mutants, with the exception of Y428F, which were scattered, were best fit with a Hill coefficient of <1, as justified by the likelihood ratio test. In a representative data set, the critical value of the test statistic was much below 0.05 (p value = 0.002). A possible origin for a nonunitary Hill coefficient is discussed later.

Approximately two-thirds of the mutations had no significant or notable effect on the affinity for ACh (K_{ACh} = 14.7 ± 0.8 mM for the wild type). Approximately one-third did and are listed in boldface. Alanine mutations of F220 and Y432 decreased affinity (K_{ACh} = 81.7 ± 5.7 and 45.3 ± 8.5 mM, respectively). Alanine mutations of W331, Y343, and Y428 also decreased affinity (K_{ACh} = 130 ± 18, 92.0 ± 6.8, and 67.1 ± 5.7 mM, respectively). Conservative mutation to F at the latter three sites resulted in affinities intermediate between those of the alanine mutants and wild type. None of the mutations increased the affinity for ACh.

Transport of [^{3}H]ACh. These data are required to determine whether a mutation that affects the ACh binding site has only a local effect or a widespread effect on the structure

Table 2: Macroscopic Parameters for Equilibrium Binding of ACh and Vesamicol[a]

	K_{ACh}[b]	H[c]	K_v[d]	B_{max}[e]
wild type	14.7 ± 0.8	0.75 ± 0.02	14.3 ± 0.5	10.1 ± 0.1
Y50A	15.4 ± 1.5	0.67 ± 0.03	13.3 ± 1.1	10.8 ± 0.2
Y50F	13.5 ± 4.2	0.78 ± 0.10	17.4 ± 2.0	10.1 ± 0.2
Y175A	20.3 ± 3.4	0.76 ± 0.06	14.5 ± 1.1	9.81 ± 0.16
Y175F	15.4 ± 2.3	0.78 ± 0.06	12.6 ± 0.7	8.54 ± 0.11
F191A	15.2 ± 1.5	0.85 ± 0.06	35.6 ± 7.7	10.7 ± 0.6
F191Y	17.0 ± 2.4	0.76 ± 0.06	14.9 ± 1.5	10.3 ± 0.3
F220A	**81.7** ± 5.7	0.79 ± 0.03	19.1 ± 1.7	16.4 ± 0.3
F220Y	21.5 ± 2.0	0.89 ± 0.06	26.3 ± 3.7	6.91 ± 0.25
F223A	14.8 ± 1.3	0.80 ± 0.04	14.2 ± 0.8	5.81 ± 0.06
F223Y	14.6 ± 1.1	0.93 ± 0.04	10.5 ± 0.6	4.68 ± 0.06
F307A	11.2 ± 1.1	0.93 ± 0.06	17.0 ± 1.4	3.53 ± 0.06
F307Y	11.4 ± 1.7	0.82 ± 0.07	16.4 ± 1.9	2.80 ± 0.06
W331A	**130** ± 18	0.96 ± 0.10	14.8 ± 2.1	4.98 ± 0.12
W331F	**74.5** ± 6.9	0.84 ± 0.05	20.8 ± 1.5	11.0 ± 0.2
F335A	15.6 ± 2.1	0.95 ± 0.08	**38.4** ± 3.1	5.02 ± 0.09
F335Y	26.2 ± 1.4	0.74 ± 0.02	14.4 ± 0.6	6.39 ± 0.06
Y343A	**92.0** ± 6.8	0.83 ± 0.03	25.8 ± 1.7	18.4 ± 0.4
Y343F	**76.7** ± 6.0	0.83 ± 0.04	23.6 ± 1.2	19.9 ± 0.3
Y428A	**67.1** ± 5.7	0.89 ± 0.05	8.03 ± 1.02	2.56 ± 0.06
Y428F	**49.4** ± 4.9	1.13 ± 0.09	22.1 ± 1.7	3.93 ± 0.08
Y432A	**45.3** ± 8.5	0.86 ± 0.10	16.1 ± 0.9	7.77 ± 0.09
Y432F	32.3 ± 6.2	0.86 ± 0.10	15.5 ± 1.1	10.5 ± 0.2

[a] Values are given to three significant figures ± one standard deviation. Parameter values at least three propagated standard deviations away from that of the wild type (calculated with eq 2) *and* 2-fold different are in boldface. [b] ACh dissociation constant (in mM). [c] Hill coefficient for ACh binding. [d] Vesamicol dissociation constant (in nM). [e] Maximal binding at a saturating vesamicol concentration (pmol of VAChT/mg). Transfection efficiency for individual experiments differed significantly. The standard deviations are values averaged according to eq 1.

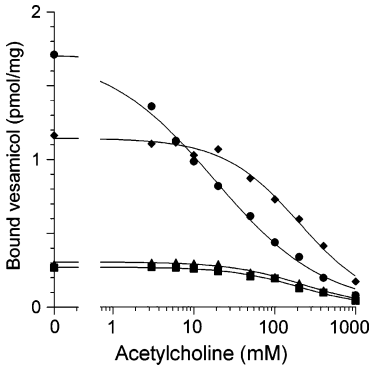

FIGURE 4: ACh affinity. Trace [^{3}H]vesamicol was displaced by the indicated concentrations of unlabeled ACh at equilibrium. Data are for representative experiments using wild-type (■), F220A (●), Y343A (▲), and W331A (◆) VAChT.

of VAChT. Such data also will identify mutants that alter only transport rates and not binding of ACh or vesamicol. Representative data are shown in Figure 5. Parameters for regression fits for the wild type and all mutated VAChTs are listed in Table 3 for (a) V_{max}/B_{max} and K_M for data exhibiting saturation and (b) $V_{max}/B_{max}/K_M$ for data not exhibiting saturation. The $V_{max}/B_{max}/K_M$ ratio is the only transport parameter that can be estimated by regression for most mutants that transport poorly. For VAChTs that transport adequately, the ratio is estimated by calculation using fitted values of V_{max}/B_{max} and K_M. $V_{max}/B_{max}/K_M$, whether obtained by regression or calculation, is the apparent second-order rate constant describing the rate of transport at subsaturating concentrations of ACh. It measures catalytic

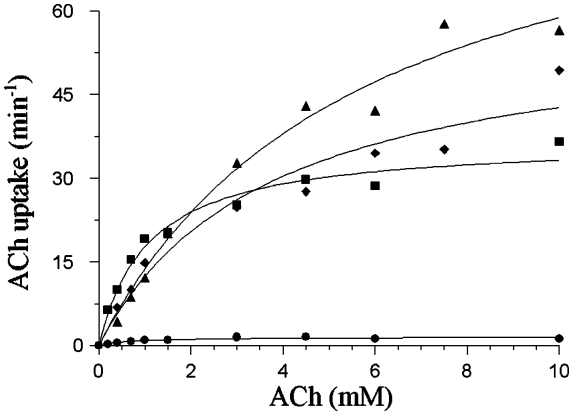

FIGURE 5: ACh transport at indicated concentrations of [^{3}H]ACh. Data were divided by the B_{max} value determined for the same preparation of the postnuclear supernatant, and the level of nonspecific binding was removed before plotting. Data are for representative experiments using wild-type (■), Y50A (●), F307A (▲), and F335A (◆) VAChT.

Table 3: Macroscopic Parameters for ACh Transport[a]

	K_M[b]	V_{max}/B_{max}[c]	$V_{max}/B_{max}/K_M$[d]
wild type	1.02 ± 0.09	21.1 ± 0.5	21.0 ± 1.9
Y50A	nd[e]	nd[e]	**0.533** ± 0.025[f]
Y50F	0.74 ± 0.18	11.8 ± 0.8	17.1 ± 3.4
Y175A	0.57 ± 0.13[g]	17.8 ± 1.0[g]	31.2 ± 7.3[g]
Y175F	0.95 ± 0.27[g]	19.7 ± 1.6[g]	20.7 ± 6.1[g]
F191A	0.94 ± 0.10	33.6 ± 0.9	35.3 ± 3.8
F191Y	0.72 ± 0.14	21.2 ± 0.8	29.3 ± 5.1
F220A	nd[e]	nd[e]	**0.370** ± 0.109[f]
F220Y	1.06 ± 0.12	28.8 ± 0.8	31.0 ± 4.7
F223A	0.98 ± 0.30	28.3 ± 1.4	33.5 ± 6.1
F223Y	1.18 ± 0.15	36.8 ± 1.2	32.1 ± 4.1
F307A	**5.34** ± 0.83	**68.1** ± 5.4	**10.1** ± 1.5
F307Y	2.54 ± 0.65	38.8 ± 3.0	17.4 ± 3.3
W331A	nd[e]	nd[e]	**2.29** ± 0.33[f]
W331F	**2.30** ± 0.28	23.2 ± 2.9	**7.05** ± 0.81
F335A	**2.79** ± 0.42	**62.1** ± 3.0	23.9 ± 2.7
F335Y	nd[e]	14.3 ± 3.4[f]	**1.22** ± 0.12[f]
Y343A	0.78 ± 0.15	20.6 ± 0.8	26.3 ± 4.6
Y343F	1.05 ± 0.18	24.4 ± 1.0	23.4 ± 3.4
Y428A	nd[e]	**9.26** ± 2.02	**2.36** ± 0.64[f]
Y428F	nd[e]	**10.7** ± 1.6	**2.66** ± 0.62[f]
Y432A	nd[e]	**4.82** ± 1.07	**1.07** ± 0.16[f]
Y432F	nd[e]	43.3 ± 12.2	**9.93** ± 2.16[f]

[a] Values are given to three significant figures ± one propagated standard deviation. Parameter values at least three propagated standard deviations away (calculated with eq 2) *and* 2-fold different from that of the wild type are in boldface. [b] Michaelis−Menten constant (in mM). [c] Maximal transport at saturating ACh concentrations normalized to B_{max} values taken from Table 2 (in min^{-1}), which is equivalent to the microscopic rate constant k_2. [d] Apparent second-order rate constant for transport at subsaturating ACh concentrations calculated from c/b if both are available or obtained from a linear fit to transport data (in mM^{-1} min^{-1}). [e] Not determined because of excessive data scatter due to poor transport. [f] Obtained from a linear fit to transport data. [g] Results from one determination.

efficacy. V_{max} in all cases was normalized to the extent of vesamicol binding (B_{max}) to correct for different expression levels. Wild-type VAChT transported ACh with a fitted K_M value of 1.02 ± 0.09 mM, a fitted V_{max}/B_{max} value of 21.1 ± 0.5 min^{-1}, and a calculated $V_{max}/B_{max}/K_M$ value of 21.0 ± 1.9 mM^{-1} min^{-1}.

One-half of the mutants exhibited no significant or notable effect on the values of macroscopic transport parameters. One-half did and are listed in boldface. Y50A and F220A mutants exhibited severely inhibited transport (0 mM^{-1} min^{-1}

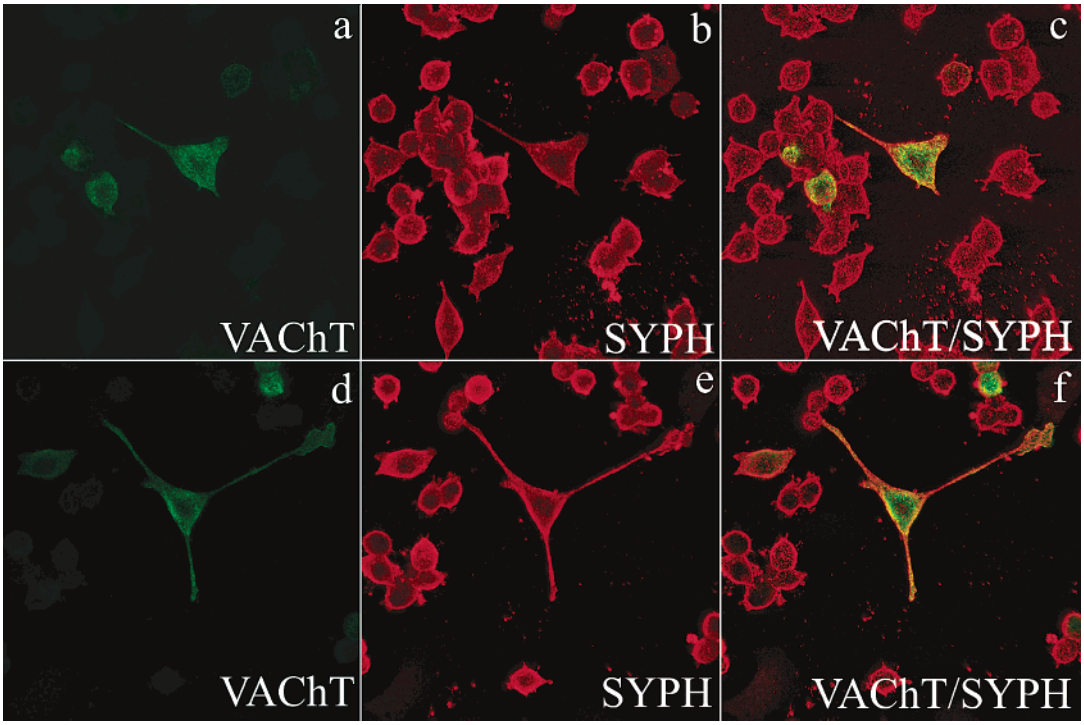

FIGURE 6: Subcellular localization of VAChT mutants. Wild-type (a−c) or Y50A mutant (d−f) VAChT immunoreactivity is green, and SYPH immunoreactivity, which is a marker of synaptic-like microvesicles, is red. VAChT is present in the cell body, near the plasma membrane, and in processes and colocalizes with SYPH in the processes and near plasma membrane (c and f). Nontransfected cells or omission of primary or secondary antibodies resulted in the expected absence of fluorescence (data not shown).

$< V_{max}/B_{max}/K_M < 1$ mM^{-1} min^{-1}). W331A, F335Y, Y428A/F, and Y432A mutants exhibited strongly inhibited transport (1 mM^{-1} min^{-1} $< V_{max}/B_{max}/K_M <$ 3 mM^{-1} min^{-1}). F307A, W331F, and Y432Y mutants exhibited moderately inhibited transport (7 mM^{-1} min^{-1} $< V_{max}/B_{max}/K_M <$ 11 mM^{-1} min^{-1}). However, this conventional measure of catalytic efficacy does not provide a comprehensive view, as F307A and F335A mutants exhibited 3-fold increased values for V_{max}/B_{max}. An increased V_{max}/B_{max} combined with an increased K_M to produce a moderately reduced or normal value for $V_{max}/B_{max}/K_M$ for these mutants. Overall, a wide variety of effects on macroscopic transport parameters was observed. The effects are interpreted mechanistically in the Discussion.

Subcellular Localization. VAChT mutants might not transport because they do not reach an acidic compartment. To test for a change in trafficking caused by a mutation, VAChT (Figure 6a,d) and SYPH (Figure 6b,e), a marker for synaptic vesicles and microvesicles, were visualized by immunofluorescence. The cells were not purposely differentiated into neuronal-like morphology, but occasionally, a successfully transfected cell spontaneously flattened and developed processes. In such cells, much punctuate staining of wild-type VAChT was near the plasma membrane in the cell body and processes and substantially colocalized with staining for SYPH. However, a significant amount of VAChT staining also was in cytoplasm where only a small amount of SYPH staining was located. Cytoplasmic staining probably arises from newly synthesized VAChT in transit to plasma membrane and microvesicles. All VAChT mutants had subcellular staining patterns similar to that of the wild type. Thus, they were targeted in a manner similar to that of the wild type.

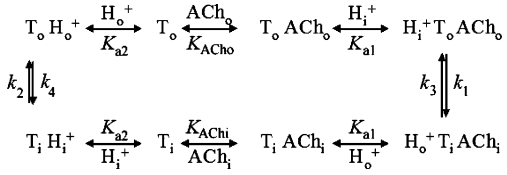

FIGURE 7: Proposed microscopic kinetic mechanism for VAChT. Two-headed arrows indicate equilibrium, whereas one-headed arrows indicate a rate step. The subscripts o and i indicate outside (cytoplasmic) and inside (luminal) locations, respectively. A transport cycle starts with VAChT species T_o and proceeds clockwise.

DISCUSSION

K_M, V_{max}/B_{max}, and K_{ACh} are macroscopic parameters that characterize aggregate properties of active transport and equilibrium binding of ACh, respectively. They do not tell us much about how VAChT works. Figure 7 shows a more informative model for the microscopic kinetics of VAChT (*47*). Such a model designates each step in the transport cycle. The cycle begins with binding of cytoplasmic ACh to outwardly oriented "site 2" with equilibrium dissociation constant K_{AChO} and protonation of inwardly oriented "site 1". Loaded VAChT translocates bound ligands across the membrane with a rate constant k_1. It then releases ACh to the inside and the proton to the outside. Unloaded, internally oriented site 2 binds a proton, after which VAChT translocates the proton across the membrane in the rate-limiting step with a rate constant k_2. The proton is released to the outside of the vesicle to complete the transport cycle (*3*). Parameters associated with each reaction arrow are termed microscopic.

The mathematical relationships between macroscopic and microscopic parameters for the model have been derived (*3*), and estimates for all parameter values have been obtained

(*46*). Because the values of microscopic parameters in additive relationships differ by large factors, the expressions simplify to $K_{ACh} \cong K_{AChO}$, $V_{max} \cong k_2 B_{max}$, and $K_M \cong (K_{AChO} k_2)/k_1$. In other words, macroscopic K_{ACh} is set primarily by microscopic K_{AChO}, macroscopic V_{max} is set primarily by microscopic k_2 (and macroscopic B_{max}), and macroscopic K_M is set primarily by microscopic K_{AChO}, k_2, and k_1. The expressions can be rearranged to compute values for k_2 and k_1, as shown in eqs 3 and 4, for which errors are propagated.

$$k_2 \pm \sigma_{k_2} = \left(\frac{V_{max}}{B_{max}}\right)\left[1 \pm \sqrt{\left(\frac{\sigma_{V_{max}}}{V_{max}}\right)^2 + \left(\frac{\sigma_{B_{max}}}{B_{max}}\right)^2}\right] \quad (3)$$

$$k_1 \pm \sigma_{k_1} = \left(\frac{k_2 K_{ACh}}{K_M}\right)\left[1 \pm \sqrt{\left(\frac{\sigma_{k_2}}{k_2}\right)^2 + \left(\frac{\sigma_{K_{ACh}}}{K_{ACh}}\right)^2 + \left(\frac{\sigma_{K_M}}{K_M}\right)^2}\right] \quad (4)$$

Separated values for V_{max}/B_{max} and K_M could not be estimated for some mutants because of poor transport. Instead, the ratio $V_{max}/B_{max}/K_M$ was estimated. Assuming that the approximations leading to eqs 3 and 4 are valid in such mutants, $V_{max}/B_{max}/K_M \cong k_1/K_{ACh}$. After rearrangement

$$k_1 \pm \sigma_{k_1} = [(V_{max}/B_{max}/K_M)K_{ACh}]\left[1 \pm \sqrt{\left(\frac{\sigma_{V_{max}/B_{max}/K_M}}{V_{max}/B_{max}/K_M}\right)^2 + \left(\frac{\sigma_{K_{ACh}}}{K_{ACh}}\right)^2}\right] \quad (5)$$

The value of k_2 cannot be estimated for poorly transporting mutants that do not exhibit saturation of transport.

K_{ACh} is simultaneously macroscopic and microscopic, and no transformation of its value is required to obtain microscopic K_{AChO}. K_v is assumed to be simultaneously macroscopic and microscopic, as vesamicol binds to inwardly and outwardly oriented VAChT with similar affinities (*46*, *48*). Potential changes in acid dissociation constants were ignored in the current work, as no mutations were introduced at ionic groups and the pH was held constant.

Because the mathematical treatment that relates macroscopic and microscopic kinetics is complex, yet critical to microscopic structure−function analysis, an intuitive, hydrodynamic mimic of transporter function has been devised (*47*). This was possible because computer simulation demonstrates that resting VAChT is distributed predominantly among the species shown along the top of Figure 7, and transporting VAChT is distributed predominantly among the species shown along the bottom. The mimic illustrates why (a) the values of K_{ACh} and K_M in the rat wild type differ from each other by ~14-fold in the current study and (b) mutations affecting different microscopic steps affect macroscopic properties of VAChT in certain ways.

Values of K_{ACh}, K_M, V_{max}/B_{max}, and $V_{max}/B_{max}/K_M$ for mutants that differ from those for the wild type (boldface in Tables 2 and 3) were analyzed with eqs 2−5. The mutant to wild-type ratios of microscopic parameters were computed with propagated errors in a manner analogous to eq 3 (except that $V_{max} \pm \sigma_{V_{max}}$ was replaced by the value of a microscopic parameter $\pm \sigma$ for a mutant and $B_{max} \pm \sigma_{B_{max}}$ was replaced by the value of the same microscopic parameter $\pm \sigma$ for the wild type). Ratios of at least 2-fold that also are at least three propagated standard deviations from 1 as computed in a manner analogous to eq 2 are listed in Table 4. An up or down arrow indicates the direction of change for the value of the mutant parameter.

Table 4: Mutant to Wild-Type Ratios of Microscopic Parameters[a]

mutant	K_{AChO}[b]	k_2[c]	k_1[d]	k_1[e]	mutant	K_{AChO}	k_2	k_1	k_1
W331A	8.9 ↑	nd[f]	nd[f]	wt[g]	Y50F	wt[g]	wt[g]	wt[g]	na[h]
W331F	5.1 ↑	wt[g]	wt[g]	na[h]	Y175A	wt[g]	wt[g]	wt[g]	na[h]
F220A	5.6 ↑	nd[f]	nd[f]	10 ↓	Y175F	wt[g]	wt[g]	wt[g]	na[h]
Y343A	6.3 ↑	wt[g]	8.0 ↑	na[h]	F191A	wt[g]	wt[g]	wt[g]	na[h]
Y343F	5.2 ↑	wt[g]	5.9 ↑	na[h]	F191Y	wt[g]	wt[g]	wt[g]	na[h]
Y428A	4.6 ↑	2.3 ↓	nd[f]	2.0 ↓	F220Y	wt[g]	wt[g]	wt[g]	na[h]
Y428F	3.4 ↑	2.0 ↓	nd[f]	2.3 ↓	F223A	wt[g]	wt[g]	wt[g]	na[h]
Y432A	3.1 ↑	4.3 ↓	nd[f]	6.3 ↓	F223Y	wt[g]	wt[g]	wt[g]	na[h]
Y50A	wt[g]	nd[f]	nd[f]	33 ↓	F307Y	wt[g]	wt[g]	wt[g]	na[h]
F307A	wt[g]	3.2 ↑	2.1 ↓	na[h]	Y432F	wt[g]	wt[g]	nd[f]	wt[g]
F335A	wt[g]	3.0 ↑	wt[g]	na[h]					
F335Y	wt[g]	wt[g]	nd[f]	10 ↓					

[a] Ratios are computed from boldface values of parameters listed in Tables 2 and 3 using eqs 2−5. The up arrow (↑) indicates an increase in the parameter value for the mutant relative to the wild type and the down arrow (↓) a decrease. Values are given to two significant figures. [b] Dissociation constant for T_oACh_o (outwardly oriented complex). [c] Rate-determining step in steady-state transport. [d] Calculated from eq 4 for mutants yielding V_{max}/B_{max} and K_M. [e] Calculated from eq 5 for poorly transporting mutants yielding only the ratio $V_{max}/B_{max}/K_M$. [f] Not determined. [g] No statistically significant or notable change from the wild-type value, meaning the ratio is close to 1. [h] Not applicable.

The goal of this approach is to identify, more precisely than is possible by analysis of macroscopic parameters alone, the roles that mutated residues play in VAChT function. For example, microscopic analysis reveals that two of the three microscopic parameters determining K_M are rate constants. Thus, mutations affecting the value of K_M cannot be assumed to be at the ACh binding site. They might be distant from the binding site but affect one of the rate constants. Mutations affecting the ACh binding site can be recognized with certainty only if they affect K_{ACh}.

Of course, conclusions about kinetics data depend on the validity of the underlying kinetics model. If the kinetics model utilized here should in the future be proved to be erroneous, the data reported here might have to be reinterpreted. Kinetics analyses do not depend on knowledge of the three-dimensional structure of the transporter.

Mutations have been divided into four groups in Table 4: a group having only decreased ACh affinity, a group having both decreased ACh affinity and an effect on at least one of the microscopic rate steps, a group having no effect on ACh affinity but an effect on at least one of the rate steps, and a group exhibiting full wild-type behavior.

The first group is restricted to mutations of residue W331. K_{AChO} was increased ~9-fold in W331A and was only partially normalized in W331F. The functional result is slower uptake at subsaturating ACh concentrations (due to weaker binding of ACh, not to slower intrinsic rates) and no change in the uptake rate at saturating ACh (which, however, occurs only at concentrations of ACh higher than those for the wild type). *In vivo*, this probably would mean less uptake, as a typical concentration of cytoplasmic ACh probably is approximately the same as wild-type K_M, or ~1 mM (*1*). Because computational studies and the frequency of occurrence in structurally defined protein−ligand complexes indicate that tryptophan is best suited for cation−π

solvation, and the W331A/F mutations have no effect on microscopic rates, W331 is a good candidate for being part of the ACh binding site.

Mutations producing mixed ACh binding and rate effects begin in Table 4 with the F220A mutant. This mutant transported very poorly because of a combined ~6-fold increase in the value of K_{ACho} and ~10-fold decrease in the value of k_1. A decrease in k_2 also might have occurred, but this could not be determined.

Y343A/F mutants exhibited 5−6-fold increased K_{ACho} values, yet K_M (and V_{max}) values were unchanged (Table 3). The functional result is no change in the uptake rate at any concentration of ACh. *In vivo*, this probably would be a null mutation. The lack of change in K_M occurred because an ~6−8-fold increase in the value of k_1 offset the increase in K_{ACho}. This example of compensation illustrates the importance of determining microscopic parameters. If the lack of change in K_M had been used to infer a lack of change in affinity for ACh, *the incorrect conclusion that Y343 is not linked to the ACh binding site would have been reached*. Because the values of k_1 increased and the values of k_2 did not change, the Y343A/F mutants differentially affected and thus resolved the microscopic rate steps from each other.

Y428A/F mutants exhibited an ~3−5-fold increase in K_{ACho}. The inability of F at this position to restore wild-type behavior suggests that the hydroxyl group plays a role in orienting Y428. These mutants also exhibited an ~2-fold decrease in values for both k_1 and k_2. Y432A behaved similarly, except that k_1 and k_2 values decreased more. The functional result of these mutations is slower uptake at all concentrations of ACh. *In vivo*, this probably would mean less uptake. Mutations at Y428 and Y432 do not resolve the microscopic rate steps from each other.

Residues having mixed ACh binding and rate effects might be at the ACh binding site, and when ACh binds, they might trigger a conformational change that is part of a microscopic rate step. On the other hand, they might be buried in VAChT at a distance from the ACh binding site, and mutation might cause a propagated conformational change that disrupts both ACh binding and rate steps. Simple solid geometry makes it unlikely that all five of the aromatic residues found here to be linked to the ACh binding site can engage in cation−π solvation. Additional work will be required to distinguish among possibilities for mutants that have mixed ACh binding and rate effects. All of the mutations reducing ACh affinity did so by amounts similar to those observed for similar mutations in nicotinic and muscarinic ACh receptors (*49*−*51*).

Mutations affecting rate steps but not ACh binding begin in Table 4 with Y50A. This mutant transported very poorly due to a 33-fold decrease in the value of k_1 (and possibly a decrease in k_2 that could not be determined).

The F307A mutation increased the value of k_2 by ~3-fold and decreased the value of k_1 by ~2-fold. This mutant thus resolves k_1 and k_2 steps from each other. Although V_{max}/B_{max} and K_M increase due to the increase in k_2, K_M increases even more due to the decrease in k_1 (Table 3). The functional result is slower uptake at subsaturating ACh concentrations and faster uptake at saturating ACh (which, however, requires higher concentrations of ACh). *In vivo*, the effect of the mutation might depend on the activity state of, and thus cytoplasmic ACh concentration in, the nerve terminus.

Mutation F335A increased the value of k_2 by ~3-fold and had no effect on the value of k_1. V_{max}/B_{max} and K_M increased by the same factor because of this (Table 3). The functional result is no change in the uptake rate at subsaturating ACh concentrations and faster uptake at saturating ACh (which, however, requires higher concentrations of ACh). *In vivo*, this might mean more uptake.

Mutation F335Y had no effect on the value of k_2 and decreased the value of k_1 by ~10-fold. The functional result is slower uptake at subsaturating ACh concentrations and no change in the uptake rate at saturating ACh (which, however, requires higher concentrations of ACh). *In vivo*, this probably would mean less uptake.

The A, F, Y substitution sequence at position 335 yielded a progression in effects on microscopic rate constants that correlates with molecular volume (*52*). Thus, for A at this position, k_1 remained at the wild-type value and k_2 increased; for F at this position, both microscopic rates are wild-type rates, and for Y at this position, k_1 decreased and k_2 remained at the wild-type value. The pattern suggests that TMD VIII has a pivotal role in both of the conformational changes that occur in the transport cycle. F335A is the only mutant to affect vesamicol affinity, causing a 2.7-fold decrease (Table 2).

Mutations that affect rate steps but not thermodynamic affinity for ACh further illustrate the importance of determining microscopic parameters. F307A and F335A (already analyzed above for other effects) exhibited increases in the value of K_M (Table 3) with no change in the value of K_{ACho} (Table 4). If the increases in K_M had been used to infer a change in ACh affinity, *the incorrect conclusion that these residues are linked to the ACh binding site would have been reached.*

All other mutants exhibited wild-type behavior. This includes Y175A/F. Y175 is conserved in VAChT and VMATs (Figure 1). Null results for Y175A/F constitute a negative control, as a residue conserved in VAChT and VMATs probably is not located at a substrate binding site.

The Hill coefficient consistently was less than 1 for displacement of bound [^{3}H]vesamicol by ACh. The apparent negative cooperativity was not caused by mutation, as the wild type and mutants share the phenomenon. It is unlikely that authentic negative cooperativity arising from a VAChT oligomer exists, as there is no evidence supporting oligomerization of VAChT. The following hypothesis seems to be reasonable. Immunocytochemistry carried out here and by other researchers demonstrates that VAChT overexpressed in PC12 cells is found in several cellular membrane types (*53*, *54*). Also, a recently developed assay that monitors transmembrane reorientation of the ACh binding site gives results consistent with the presence of transporting and nontransporting VAChT in the type of preparation used here, plausibly because some of the VAChT is not present in an acidic compartment (*48*). Different lipid compositions in different membrane types might affect the conformation of the ACh binding site differentially to generate different affinities that will appear as negative cooperativity. Functional VAChT apparently is homogeneous, as regression to transport data obtained with expressed rat VAChT and natural *Torpedo* VAChT in synaptic vesicles does not require a Hill coefficient different from unity (*46*).

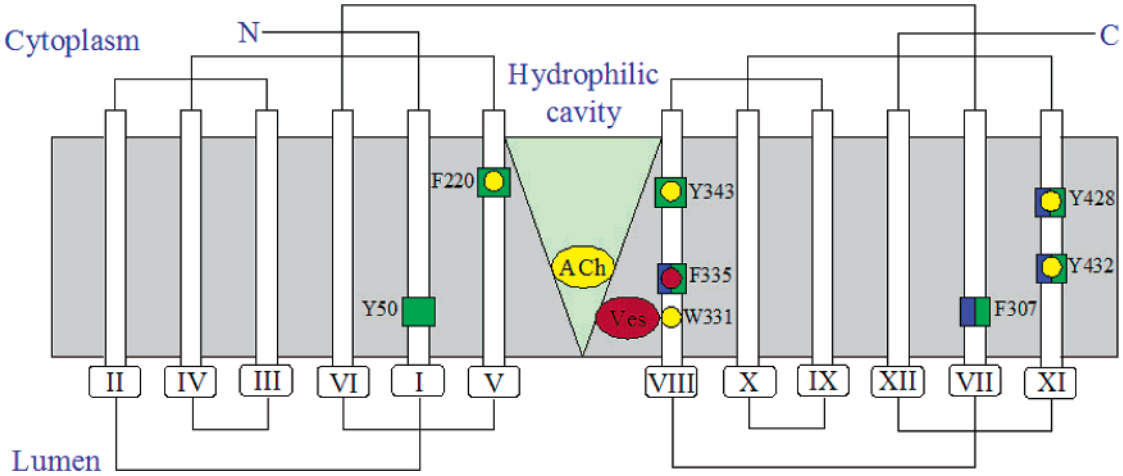

FIGURE 8: Mapping of VAChT mutants into the LacY structure. TMDs are denoted with Roman numerals. The approximate positions of residues in VAChT yielding ACh affinity, vesamicol affinity, and rate effects when mutated are mapped into the cartoon. A yellow circle indicates an ACh affinity effect. The red circle indicates a vesamicol affinity effect. A green rectangle indicates a k_1 effect, and a blue rectangle indicates a k_2 effect. The figure ignores tilts and kinks in helices and is adapted from Abramson *et al.* (*61*).

ACh and choline binding sites tend not to be completely buried, which reflects the cationic character of the ligand. However, they are not extensively exposed to water because of the aromatic component of the cation−π complex (*55*). In addition to cation−π solvation, other interactions between bound ACh and the binding site surely are present, like a hydrogen bond to the ester carbonyl.

VAChT also transports ACh analogues, including many that increase the steric bulk around the quaternary nitrogen (*45*, *56*). Cation−π solvation can adapt to different substrate shapes through induced fit. Thus, rotations about the β-carbon can allow substantial change in the position of π-electrons in aromatic side chains without distortion of the polypeptide backbone. Similar induced-fit models have been proposed to explain the ability of AChE (*24*), liver X receptor β (*57*), and the multidrug resistance protein MRP1 (*58*) to bind wide ranges of ligands. In addition, aromatic side chains at the protein−water interface in other regions of VAChT might (a) provide a "slide guide" that increases the rate of diffusion of ACh to its binding site and (b) act as a gate or filter for ACh (*59*).

Many of the current results confirm previous conclusions that the ACh and vesamicol binding sites are not identical to each other (*37*, *46*). The first is that regression to data for vesamicol binding does not require a Hill coefficient different from unity. The second is that eight mutants decreased ACh affinity without any effect on vesamicol affinity, whereas one mutant decreased vesamicol affinity without any effect on ACh affinity.

VAChT is a member of the large, major facilitator superfamily (MFS) defined by sequence homology (*60*). The three-dimensional structures of three MFS proteins recently were determined: the *E. coli* lactose permease [LacY, PDB entry 1pv6 (*61*)], the *Oxalobacter formigenes* oxalate transporter [OxlT (*62*, *63*)], and the *E. coli* glycerol-3-phosphate/inorganic phosphate antiporter [GlpT, PDB entry 1pw4 (*64*)]. Supersecondary structures in these transporters are highly similar. Hirai *et al.* (*65*) propose that most prokaryotic and eukaryotic members of the MFS have a similar packing scheme for TMDs.

The determined structures contain 12 TMD helices organized into two halves related by approximate internal 2-fold symmetry. Many of the helices are tilted away from the perpendicular and contain kinks. All three transporter structures exhibit a large, putative, central transport channel that is (a) open on the cytoplasmic face, (b) closed on the extracytoplasmic face, and (c) lined at different depths by TMD helices I, II, IV, V, VII, VIII, X, and XI. The substrate binding site in LacY is composed of residues projecting into the transport channel from TMDs I, IV, V, VII, and XI, and in GlpT, it is composed of residues from TMDs I, V, and VII.

Although the amount of data allowing comparison of TMD packing in VAChT with that in determined MFS structures is limited, sequence homology and available ion pairing inferences are consistent with similar packing relationships (*66*). Thus, the structure of LacY, which is the most studied member of the MFS, will be used here as a template to localize residues mutated in the current study (Figure 8). The locations might have to be revised as more becomes known about VAChT structure.

The three TMDs containing residues implicated in ACh binding (V, VIII, and XI) line the putative transport channel. However, TMD VIII is not involved in substrate binding in determined structures, and it lines the channel only close to the vesicular lumen. The one VAChT residue implicated exclusively in ACh binding (W331) is in the beginning of TMD VIII and thus close to the vesicular lumen. The ACh binding site probably is located deep in the transport channel, away from the bulk cytoplasm, for this reason. The vesamicol binding site probably is located close to but not coincident with the ACh binding site for the reasons cited above. The other residue in TMD VIII implicated in ACh binding (Y343) is linked in addition to the k_1 rate step. Because it is located further along TMD VIII than W331 is, Y343 probably is proximal to the cytoplasm. In an alternating access model of transport, the k_1 step requires residues proximal to the cytoplasm to close the transport channel behind bound ACh as residues proximal to the vesicular lumen open the transport channel in front of bound ACh. The geometry shown in Figure 8 accommodates this requirement and rationalizes the binding and rate effects caused by mutations of W331 and Y343.

A number of mutations resolved the microscopic rate steps from each other, which suggests that different parts of VAChT control rate steps. These mutations present an interesting topology. Most mutations slowing the k_1 step lie in symmetrically related TMDs I and VII (Y50A and F307A) and symmetrically related TMDs V and XI (F220A, Y428A/F, and Y432A). Most mutations affecting the k_2 step lie in TMDs VII and XI (F307A, Y428A/F, and Y432A). Four mutations in TMD VIII (F335A/Y and Y343A/F) are linked to either the k_1 or k_2 rate step.

In summary, values for microscopic parameters that characterize major steps in the VAChT transport cycle can be extracted from macroscopic data. Many of the mutations are pleiotropic, and microscopic apportionment of changes to ACh binding and transport rate steps is important to unraveling true effects. Mutation of residue W331, which lies in the beginning of TMD VIII proximal to the vesicular lumen, produced 5- and 9-fold decreased ACh affinity and no change in other parameters. This residue is a good candidate for cation−π solvation of bound ACh. Mutation of four other residues decreased ACh affinity up to 6-fold and also affected microscopic rate constants. The roles of these residues in ACh binding and transport thus are complex. Nine mutations resolved the ACh and vesamicol binding sites from each other. Other mutations affected only the rates of the transmembrane reorientation steps, and four mutations *increased* the rate of one or the other. Two mutations increased the value of K_M up to 5-fold due to rate effects with no effect on ACh affinity.

ACKNOWLEDGMENT

We thank Dr. Louis Hersh for a gift of the PC12$^{A123.7}$ cell line and Dawn T. Bravo for the recombinant expression vector. We are especially thankful to Dr. Brian Matsumoto (University of California, Santa Barbara, CA) for carrying out confocal microscopy.

REFERENCES

1. Parsons, S. M., Prior, C., and Marshall, I. G. (1993) Acetylcholine transport, storage, and release, *Int. Rev. Neurobiol. 35*, 279−390.
2. Usdin, T. B., Eiden, L. E., Bonner, T. I., and Erickson, J. D. (1995) Molecular biology of the vesicular ACh transporter, *Trends Neurosci. 18*, 218−224.
3. Nguyen, M. L., Cox, G. D., and Parsons, S. M. (1998) Kinetic parameters for the vesicular acetylcholine transporter: two protons are exchanged for one acetylcholine, *Biochemistry 37*, 13400−13410.
4. Alfonso, A., Grundahl, K., Duerr, J. S., Han, H.-P., and Rand, J. B. (1993) The *Caenorhabditis elegans* unc-17 gene: a putative vesicular acetylcholine transporter, *Science 261*, 617−619.
5. Erickson, J. D., Varoqui, H., Schäfer, M. K.-H., Modi, W., Diebler, M.-F., Weihe, E., Rand, J., Eiden, L. E., Bonner, T. I., and Usdin, T. B. (1994) Functional identification of a vesicular acetylcholine transporter and its expression from a "cholinergic" gene locus, *J. Biol. Chem. 269*, 21929−21932.
6. Roghani, A., Feldman, J., Kohan, S. A., Shirzadi, A., Gundersen, C. B., Brecha, N., and Edwards, R. H. (1994) Molecular cloning of a putative vesicular transporter for acetylcholine, *Proc. Natl. Acad. Sci. U.S.A. 91*, 10620−10624.
7. Varoqui, H., Diebler, M.-F., Meunier, F.-M., Rand, J. B., Usdin, T. B., Bonner, T. I., Eiden, L. E., and Erickson, J. D. (1994) Cloning and expression of the vesamicol binding protein from the marine ray *Torpedo*. Homology with the putative vesicular acetylcholine transporter UNC-17 from *Caenorhabditis elegans*, *FEBS Lett. 342*, 97−102.
8. Varoqui, H., and Erickson, J. D. (1996) Active transport of acetylcholine by the human vesicular acetylcholine transporter, *J. Biol. Chem. 271*, 27229−27232.
9. Naciff, J. M., Misawa, H., and Dedman, J. R. (1997) Molecular characterization of the mouse vesicular acetylcholine transporter gene, *NeuroReport 8*, 3467−3473.
10. Kitamoto, T., Wang, W., and Salvaterra, P. M. (1998) Structure and organization of the *Drosophila* cholinergic locus, *J. Biol. Chem. 273*, 2706−2713.
11. Takamura, K., Egawa, T., Ohnishi, S., Okada, T., and Fukuoka, T. (2002) Developmental expression of ascidian neurotransmitter synthesis genes. I. Choline acetyltransferase and acetylcholine transporter genes, *Dev. Genes Evol. 212*, 50−53.
12. Spafford, J. D., Munno, D. W., van Nierop, P., Feng, Z.-P., Jarvis, S. E., Gallin, W. J., Smit, A. B., Zamponi, G. W., and Syed, N. I. (2003) Calcium channel structural determinants of synaptic transmission between identified invertebrate neurons, *J. Biol. Chem. 278*, 4258−4267.
13. Shepodd, T. J., Petti, M. A., and Dougherty, D. A. (1986) Tight, oriented binding of an aliphatic guest by a new class of water-soluble molecules with hydrophobic binding sites, *J. Am. Chem. Soc. 108*, 6085−6087.
14. Dougherty, D. A., and Stauffer, D. A. (1990) Acetylcholine binding by a synthetic receptor: implications for biological recognition, *Science 250*, 1558−1560.
15. Ma, J. C., and Dougherty, D. A. (1997) The cation-π interaction, *Chem. Rev. 97*, 1303−1324.
16. Mecozzi, S., West, A. P., Jr., and Dougherty, D. A. (1996) Cation-π interactions in aromatics of biological and medicinal interest: electrostatic potential surfaces as a useful qualitative guide, *Proc. Natl. Acad. Sci. U.S.A. 93*, 10566−10571.
17. Kumpf, R. A., and Dougherty, D. A. (1993) A mechanism for ion selectivity in potassium channels: computational studies of cation-π interactions, *Science 261*, 1708−1710.
18. Sunner, J., Nishizawa, K., and Kebarle, P. (1981) Ion−solvent molecule interactions in the gas phase. The potassium ion and benzene, *J. Phys. Chem. 85*, 1814−1820.
19. Dougherty, D. A. (1996) Cation-π interactions in chemistry and biology: a new view of benzene, Phe, Tyr, and Trp, *Science 271*, 163−168.
20. Stauffer, D. A., Barrans, R. E., and Dougherty, D. A. (1990) Concerning the thermodynamics of molecular recognition in aqueous and organic media. Evidence for significant heat capacity effects, *J. Org. Chem. 55*, 2762−2767.
21. Shepodd, T. J., Petti, M. A., and Dougherty, D. A. (1988) Molecular recognition in aqueous media: donor−acceptor and ion−dipole interactions produce tight binding for highly soluble guests, *J. Am. Chem. Soc. 110*, 1983−1985.
22. Novotny, J., Bruccoleri, R. E., and Saul, F. A. (1989) On the attribution of binding energy in antigen−antibody complexes McPC 603, D1.3, and HyHEL-5, *Biochemistry 28*, 4735−4749.
23. Sussman, J. L., Harel, M., Frolow, F., Oefner, C., Goldman, A., Toker, L., and Silman, I. (1991) Atomic structure of acetylcholinesterase from *Torpedo californica*: a prototypic acetylcholine-binding protein, *Science 253*, 872−879.
24. Harel, M., Schalk, I., Ehret-Sabatier, L., Bouet, F., Goeldner, M., Hirth, C., Axelsen, P. H., Silman, I., and Sussman, J. L. (1993) Quaternary ligand binding to aromatic residues in the active-site gorge of acetylcholinesterase, *Proc. Natl. Acad. Sci. U.S.A. 90*, 9031−9035.
25. Brejc, K., van Dijk, W. J., Klaassen, R. V., Schuurmans, M., van der Oost, J., Smit, A. B., and Sixma, T. K. (2001) Crystal structure of an ACh-binding protein reveals the ligand-binding domain of nicotinic receptors, *Nature 411*, 269−276.
26. Kao, P. N., Dwork, A. J., Kaldany, R.-R., Silver, M. L., Wideman, J., Stein, S., and Karlin, A. (1984) Identification of the α subunit half-cystine specifically labeled by an affinity reagent for the acetylcholine receptor binding site, *J. Biol. Chem. 259*, 11662-11665.
27. Galzi, J. L., Revah, F., Black, D., Goeldner, M., Hirth, C., and Changeux, J.-P. (1990) Identification of a novel amino acid α-tyrosine 93 within the cholinergic ligands-binding sites of the acetylcholine receptor by photoaffinity labeling. Additional evidence for a three-loop model of the cholinergic ligands-binding sites, *J. Biol. Chem. 265*, 10430−10437.
28. Miyazawa, A., Fujiyoshi, Y., Stowell, M., and Unwin, N. (1999) Nicotinic acetylcholine receptor at 4.6 Å resolution: transverse tunnels in the channel wall, *J. Mol. Biol. 288*, 765−786.

29. Schiefner, A., Breed, J., Bösser, L., Kneip, S., Gade, J., Holtmann, G., Diederichs, K., Welte, W., and Bremer, E. (2003) Cation-π interactions as determinants for binding of the compatible solutes glycine betaine and proline betaine by the periplasmic ligand-binding protein ProX from *Escherichia coli*, *J. Biol. Chem. 279*, 5588−5596.
30. Borges-Walmsley, M. I., McKeegan, K. S., and Walmsley, A. R. (2003) Structure and function of efflux pumps that confer resistance to drugs, *Biochem. J. 376*, 313−338.
31. Mavri, J., and Hadži, D. (2001) Modelling of ligand-receptor interactions: *ab initio* and DFT calculations of solvent reaction field effects on methylated ammonium-π and -acetate complexes, *THEOCHEM 540*, 251−255.
32. Ginty, D., Glowacka, D., DeFranco, C., and Wagner, J. (1991) Nerve growth factor-induced neuronal differentiation after dominant repression of both type I and type II cAMP-dependent protein kinase activities, *J. Biol. Chem. 266*, 15325−15333.
33. Inoue, H., Li, Y. P., Wagner, J. A., and Hersh, L. B. (1995) Expression of the choline acetyltransferase gene depends on protein kinase A activity, *J. Neurochem. 64*, 985−990.
34. Shimojo, M., Wu, D., and Hersh, L. B. (1998) The cholinergic gene locus is coordinately regulated by protein kinase A II in PC12 cells, *J. Neurochem. 71*, 1118−1126.
35. Bonzelius, F., Herman, G. A., Cardone, M. H., Mostov, K. E., and Kelly, R. B. (1994) The polymeric immunoglobulin receptor accumulates in specialized endosomes but not synaptic vesicles within the neurites of transfected neuroendocrine PC12 cells, *J. Cell Biol. 127*, 1603−1616.
36. Ojeda, A. M., Bravo, D. T., Hart, T. L., and Parsons, S. M. (2003) Equilibrium binding and transport studies, *Methods Mol. Biol. 227*, 155−177.
37. Kim, M.-H., Lu, M., Lim, E.-J., Chai, Y.-G., and Hersh, L. B. (1999) Mutational analysis of aspartate residues in the transmembrane regions and cytoplasmic loops of rat vesicular acetylcholine transporter, *J. Biol. Chem. 274*, 673−680.
38. Cox, D. R., and Hinkley, D. V. (1974) Significance tests: simple null hypothesis, in *Theoretical Statistics*, 1st ed., pp 88−130, Halsted Press, New York.
39. Seber, G. A. F., and Wild, C. J. (1989) Statistical inference, in *Nonlinear Regression*, 1st ed., pp 191−269, John Wiley & Sons, New York.
40. Rai, M., and Padh, H. (2001) Expression systems for production of heterologous proteins, *Curr. Sci. 80*, 1121−1128.
41. Bahr, B. A., and Parsons, S. M. (1986) Acetylcholine transport and drug inhibition kinetics in *Torpedo* synaptic vesicles, *J. Neurochem. 46*, 1214−1218.
42. Bahr, B. A., and Parsons, S. M. (1986) Demonstration of a receptor in *Torpedo* synaptic vesicles for the acetylcholine storage blocker L-*trans*-2-(4-phenyl[3,4-^{3}H]-piperidino) cyclohexanol, *Proc. Natl. Acad. Sci. U.S.A. 83*, 2267−2270.
43. Rogers, G. A., Parsons, S. M., Anderson, D. C., Nilsson, L. M., Bahr, B. A., Kornreich, W. D., Kaufman, R., Jacobs, R. S., and Kirtman, B. (1989) Synthesis, *in vitro* acetylcholine-storage-blocking activities, and biological properties of derivatives and analogues of *trans*-2-(4-phenylpiperidino)cyclohexanol (vesamicol), *J. Med. Chem. 32*, 1217−1230.
44. Rogers, G. A., and Parsons, S. M. (1989) Inhibition of acetylcholine storage by acetylcholine analogs *in vitro*, *Mol. Pharmacol. 36*, 333−341.
45. Clarkson, E. D., Rogers, G. A., and Parsons, S. M. (1992) Binding and active transport of large analogues of acetylcholine by cholinergic synaptic vesicles *in vitro*, *J. Neurochem. 59*, 695−700.
46. Bahr, B. A., Clarkson, E. D., Rogers, G. A., Noremberg, K., and Parsons, S. M. (1992) A kinetic and allosteric model for the acetylcholine transporter-vesamicol receptor in synaptic vesicles, *Biochemistry 31*, 5752−5762.
47. Bravo, D., and Parsons, S. M. (2002) Microscopic kinetics and structure−function analysis in the vesicular acetylcholine transporter, *Neurochem. Int. 41*, 285−289.
48. Bravo, D. T., Kolmakova, N. G., and Parsons, S. M. (2004) Transmembrane reorientation of the substrate binding site in vesicular acetylcholine transporter, *Biochemistry 43*, 8787−8793.
49. Sullivan, D., Chiara, D. C., and Cohen, J. B. (2002) Mapping the agonist binding site of the nicotinic acetylcholine receptor by cysteine scanning mutagenesis: antagonist footprint and secondary structure prediction, *Mol. Pharmacol. 61*, 463−472.
50. Ward, S. D. C., Curtis, C. A. M., and Hulme, E. C. (1999) Alanine-scanning mutagenesis of transmembrane domain 6 of the m_1 muscarinic acetylcholine receptor suggests that Tyr381 plays key roles in receptor function, *Mol. Pharmacol. 56*, 1031−1041.
51. Wess, J., Maggio, R., Palmer, J., and Vogel, Z. (1992) Role of conserved threonine and tyrosine residues in acetylcholine binding and muscarinic receptor activation. A study with m3 muscarinic receptor point mutants, *J. Biol. Chem. 267*, 19313−19319.
52. Tsai, J., Taylor, R., Chothia, C., and Gerstein, M. (1999) The packing density in proteins: standard radii and volumes, *J. Mol. Biol. 290*, 253−266.
53. Liu, Y., and Edwards, R. H. (1997) Differential localization of vesicular acetylcholine and monoamine transporters in PC12 cells but not CHO cells, *J. Cell Biol. 139*, 907−916.
54. Krantz, D. E., Waites, C., Oorschot, V., Liu, Y., Wilson, R. I., Tan, P. K., Klumperman, J., and Edwards, R. H. (2000) A phosphorylation site regulates sorting of the vesicular acetylcholine transporter to dense core vesicles, *J. Cell Biol. 149*, 379−395.
55. Gallivan, J. P., and Dougherty, D. A. (2000) A computational study of cation-π interactions *vs* salt bridges in aqueous media: implications for protein engineering, *J. Am. Chem. Soc. 122*, 870−874.
56. Kim, M. H., Lu, M., Rogers, G. A., Parsons, S. M., and Hersh, L. B. (2003) Specificity of the rat vesicular acetylcholine transporter, *Neurochem. Res. 28*, 473−476.
57. Färnegårdh, M., Bonn, T., Sun, S., Ljunggren, J., Ahola, H., Wilhelmsson, A., Gustafsson, J.-A., and Carlquist, M. (2003) The three-dimensional structure of the liver X receptor β reveals a flexible ligand binding pocket that can accommodate fundamentally different ligands, *J. Biol. Chem. 278*, 38821−38828.
58. Campbell, J. D., Koike, K., Moreau, C., Sansom, M. S. P., Deeley, R. G., and Cole, S. P. C. (2004) Molecular modeling correctly predicts the functional importance of Phe^{594} in transmembrane helix 11 of the multidrug resistance protein, MRP1 (ABCC1), *J. Biol. Chem. 279*, 463−468.
59. Tang, Y., Zaitseva, F., Lamb, R. A., and Pinto, L. H. (2002) The gate of the influenza virus M_2 proton channel is formed by a single tryptophan residue, *J. Biol. Chem. 277*, 39880−39886.
60. Linial, M. (1993) Vesicular transporters join the major facilitator superfamily (MFS), *Trends Biochem. Sci. 18*, 248−249.
61. Abramson, J., Smirnova, I., Kasho, V., Verner, G., Kaback, H. R., and Iwata, S. (2003) Structure and mechanism of the lactose permease of *Escherichia coli*, *Science 301*, 610−615.
62. Hirai, T., Heymann, J. A. W., Shi, D., Sarker, R., Maloney, P. C., and Subramaniam, S. (2002) Three-dimensional structure of a bacterial oxalate transporter, *Nat. Struct. Biol. 9*, 597−600.
63. Heymann, J. A. W., Hirai, T., Shi, D., and Subramaniam, S. (2003) Projection structure of the bacterial oxalate transporter OxlT at 3.4 Å resolution, *J. Struct. Biol. 144*, 320−326.
64. Huang, Y., Lemieux, M. J., Song, J., Auer, M., and Wang, D.-N. (2003) Structure and mechanism of the glycerol-3-phosphate transporter from *Escherichia coli*, *Science 301*, 616−620.
65. Hirai, T., Heymann, J. A. W., Maloney, P. C., and Subramaniam, S. (2003) Structural model for 12-helix transporters belonging to the major facilitator superfamily, *J. Bacteriol. 185*, 1712−1718.
66. Parsons, S. M. (2000) Transport mechanisms in acetylcholine and monoamine storage, *FASEB J. 14*, 2423−2434.

BI049562B